Stress orientation and relativistic effects on the separation of moving screw dislocations

Z. Q. Wang* and I. J. Beyerlein
Theoretical Division, Los Alamos National Laboratory, Los Alamos, New Mexico 87545, USA
(Received 28 January 2008; revised manuscript received 3 April 2008; published 15 May 2008)

The subsonic motion of a fast-moving, extended screw dislocation in an fcc metal under constant stress is studied using continuum linear elastic dislocation theory and molecular dynamics (MD) simulation. In this regime, many phenomena predicted by the theory are shown to prevail in simulation, in particular, relativistic effects and stress orientation effects. Due to the former, the fault width is found to contract as it moves faster until ≈80% of the shear wave speed, beyond which a turning point occurs preventing it from constricting to a perfect one as speed increases further. The stress orientation effect, which is first introduced by Nabarro [Philos. Mag. **14**, 861 (1966)], is demonstrated here to manifest when the shear stress resolved in the direction of motion and glide plane becomes high. A simple analytical expression for the steady-state fault width accounting for both stress orientation and relativistic effects is presented. In MD simulation under arbitrary stress states, both the dislocation velocity and separation width achieve a quasisteady state, about which they oscillate with an amplitude and frequency that reduces with speed. The separation width oscillates about a value close to that predicted by the new analytical expression. The drag coefficient is found to linearly increase with speed for speeds greater than 20% of the shear wave speed.

DOI: 10.1103/PhysRevB.77.184112 PACS number(s): 61.72.Bb, 61.72.Lk

I. INTRODUCTION

Dislocations in fcc metals can find it energetically favorable to dissociate into two partial dislocations with a stacking fault in between (Fig. 1).[1] The stress-free stacking fault width, w_0, is determined by a balance between the stacking fault energy and the elastic interaction energy.[1,2] Accordingly, w_0 is a function of the stacking fault energy γ, elastic properties of the crystal, and dislocation character (e.g., edge, screw, and mixed).[3] However, in the presence of a stress field, the actual stacking fault width w may either contract or expand from w_0. If the orientation of the stress is such that the force transverse to the dislocation line is higher on the leading partial than that on the trailing partial, then $w > w_0$. Conversely, when the transverse force on the trailing partial is higher, then $w < w_0$. This stress orientation effect was first noted by Nabarro.[4]

Copley and Kear[5] studied the stress orientation effect on w of a moving dislocation and demonstrated that it is pronounced only at high applied stresses and for certain crystallographic orientations. Their equation of motion made use of the difference in Schmid factors between the partials and an exponential law to relate stress to dislocation velocity. At such high stresses, however, the exponential stress-velocity relationship no longer applies, and many effects not included in their formulation, such as inertia, relativistic effects, and dislocation drag, become important and will affect the prediction of w. The equation of motion for an extended dislocation including linear drag, instead of the exponential stress-velocity law, can be found in the work of Hirth and Lothe.[3] There, they used Peach-Koehler (PK) forces on each partial in the direction of motion rather than their Schmid factors. As proven by Nabarro,[4,6] a PK or Schmid-factor-based formulation will not lead to fundamentally different results.

The stress orientation effect was later used by Bonneville and Escaig[7] to study the propensity of cross slip. A stacking fault width is then assumed to narrow or widen based on the sign of the shear stress resolved normal to the dislocation line and in its glide plane, the so-called "edge" shear stress. With this, they presented the "narrowing-widening" concept for cross slip: An orientation favors cross slip when a dislocation narrows on its primary plane and widens on its cross-slip plane. The stresses or velocities required to invoke a significant stress orientation effect were not addressed and w was not directly calculated.

In the aforementioned studies, dislocation speed v either had no effect on w or, through a direct relationship with stress, had an effect interchangeable with stress. This assumption works well for low dislocation velocities. At high velocities (beyond 10–20% shear wave speed), relativistic effects, inertial effects, and changes in mobility coefficient become important, which causes v to have a separate influence on w from stress. Early work[8–11] showed that fast-moving dislocations exhibited so-called "relativistic effects" as their speeds approached the shear wave speed C, drawing an analogy to Einstein's theory of relativity for particles approaching the speed of light. Their impact on the interaction

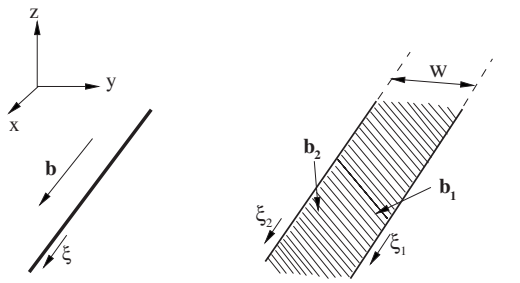

FIG. 1. Dissociation of a perfect screw dislocation into two partials separated by a stacking fault of width w.

forces and energies between two fast-moving dislocations was calculated by Weertman[8] and Hirth and Lothe[12] using different treatments. The latter Lagrangian formulation was specifically applied to study w between partials in fcc and bcc metals. Relevant to the present work, they showed that a screw dislocation in an fcc metal constricts with increasing speed until it reaches $0.8C$ (where C is the transverse sound speed) after which it expands again and eventually splits apart at speed C. In these works, only the steady-state solutions were provided, and no other forces on the dislocations, such as applied forces and friction forces, were considered. Later, the full dynamical equation of motion was presented in the work of Hirth *et al.*,[13] where the effective masses of screw and edge dislocations as a function of v were derived. In the work of Gilman,[14] inertial effects were considered. He argued that kinetic energy can be used by a moving pair of partials to shrink w, overcoming the interaction energy between them. He used a straightforward energy balance between the kinetic energy and self-energies of the two partials to estimate that the w for Cu will constrict at a speed of $C/9$. Stress orientation and relativistic effects were not considered.

The partial separation of extended dislocations can affect many aspects of dislocation behavior and hence deformation of single crystals and polycrystals. The stacking fault energy (or w_0) is a material property that distinguishes its behavior from other fcc metals. Stacking fault widths affect the activation barriers for processes that require constriction, such as cross slip,[15–20] junction intersections,[21] and climb. Cross slip, in particular, is well known to affect workhardening,[22–24] especially in stage III, substructure formation,[25,26] shape and size of the plastic zone ahead of a crack tip,[27] and response under strain reversals,[28,29] to name a few. The reaction products between extended dislocations are different than those between perfect ones,[3,23,30,31] which again can impact workhardening, particularly in reversals of low stacking fault energy materials, such as α brass.[29] When partial separations become large, such as in high-stress or high-strain rate situations, sheets of stacking faults[32,33] can be generated. Free partials can also possibly lead to twin formation through several mechanisms.[3,34–37]

In recent years, three-dimensional (3D) discrete dislocation dynamics (DD) simulations have been developed and applied to study the deformation of materials. With 3D DD, one can directly examine the motion and interaction of many dislocations, and relate microstructural evolution to the macroscopic properties of materials.[38–40] In the parametric DD formulation of Ghoniem *et al.*,[39] dislocations are modeled as curved lines between nodal points. At any instant in the deformation, the local stress $\boldsymbol{\tau}$, velocity $\mathbf{v}$, and orientation ξ of each dislocation segment can be calculated as a result of the applied stress and internal stresses due to interactions with surrounding dislocations. Dislocation multiplication from pinned sources and reactions, such as annihilation and junction formation, are included. Recently, the effects of introducing dislocation inertia and cross slip into the computational model were studied.[22,40] Inertial effects are shown to impact predictions for rates of 10^3 s^{-1} and higher (up to 10^6 s^{-1}).[40] Cross slip also greatly affected the predictions and in Ref. 22, its influence on the velocity distributions, stress-strain response, slip activity, and microstructural evolution was carefully examined. The energetic criterion for cross slip, however, did not consider w and therefore cannot appreciate the stress orientation effect, which is predicted to manifest under high-stress (high-rate) conditions.[5]

In 3D DD simulations, the dislocations are perfect. Consequently, many of the elementary dislocation processes mentioned above, which depend on dislocation core structures, dislocation dissociations, and width sizes, are neglected. Accounting for stacking fault width, for example, in the energetics of cross slip and dislocation reaction, would greatly improve the predictive capability of DD simulations. For doing so, the simplicity of the analytical expressions from two-dimensional (2D) dislocation theory, such as those found by Copley and Kear[5] and Hirth and Lothe[12] for w, is particularly attractive. However, certain behaviors of w predicted from this theory, namely, stress orientation effects, relativistic effects, stress-velocity relationships, elastic anisotropy effects, limiting speeds, and limiting separations, have yet to be validated. Atomistic simulations are well suited for studying such local behaviors and interactions between a few dislocations, as well as providing an alternative method for testing the regimes of validity of dislocation theory.

Recently, a small number of studies have applied atomistic simulation to study the changes in stacking fault width. Aubry and Hughes[41] studied the reduction in the static stacking fault width due to internal stress fields, which they experimentally observed. Mordehai *et al.*[42] carried out molecular dynamics (MD) simulations on moving screw dislocations under a widening stress state, showing that the stacking fault width periodically oscillates. These oscillations were found to reduce with dislocation speed and not depend on temperature. Duesbery[43] used a 2D atomistic model to simulate the constriction process of a screw dislocation under a narrowing stress state. The separation was found to contract at a slower rate than that predicted by an analytic elastic model (details of which were not provided). However, it is uncertain if the system was allowed to reach steady state at each stress state in loading and unloading in their simulation, which is usually assumed in theory. In the above works,[42–44] the initial partial separation of a stationary dislocation in simulation was much larger than that from 2D dislocation theory. In a recent MD study of KCl, Kinoshita *et al.*[45] observed partial separation of edge dislocations when shock compressed along the [111], but not along the [100] and [110] directions, suggesting stress orientation effects. MD simulations were used in Ref. 46 to explain the observed expansion or contraction of extended dislocations intersecting a free surface. Near the surface, a dislocation will rotate to screw orientation, thereby changing the interaction energy and hence partial separation. Many other MD simulations observe emission of partials (and deformation twins) from grain boundaries[35–37] and have demonstrated that the creation of stacking faults depends on loading rates[33] and impact velocity.[47]

In this paper, MD simulations and 2D dislocation theory are combined to study the effects of orientation, stress, and velocity on the stacking fault width of a moving screw dislocation. We begin with a review of straight dislocation theory for extended partial dislocations in fcc materials and then present the full dynamical equation of motion, including

inertia, applied stress, dislocation drag, and relativistic effects. From this, a simple expression for the steady-state w_{ss} including relativistic effects, which applies to a dislocation of any character (edge, screw, and mixed), is developed. Due to an interest in cross slip and high-rate deformation, MD simulations of a moving extended screw dislocation in copper under various high-stress states are performed. The MD simulations show that the 2D dislocation theory can reasonably predict the stress orientation effect and that this effect manifests at only high stresses.[5] It also shows that at these same high-stress conditions, relativistic effects are also important and our improved analytical formulation proves to be more accurate. The stress orientation effect has significant implications on deformations involving strain path changes and so additional MD simulations are performed for a reversal path change. Before concluding, we return to the cross-slip analysis of Bonneville and Escaig[7] and study the implications of relativistic effects on cross slip.

II. STRAIGHT DISLOCATION THEORY FOR AN EXTENDED DISLOCATION

A. Equations of motion

Consider a perfect dislocation with Burgers vector $\mathbf{b}$ and dislocation line ξ (along x) that dissociates in its slip plane (with normal along z) into two partials with Burgers vectors $\mathbf{b}_1$ and $\mathbf{b}_2$, both with the same dislocation line as the parent ξ. The dislocation moves normal to its ξ and movement along y is considered. The full equation of motion in the y direction for the two partials is

$$F_1(v) = -Bv_{1y} + F_{\mathrm{PK},1y} + f_r - \gamma, \tag{1}$$

$$F_2(v) = -Bv_{2y} + F_{\mathrm{PK},2y} - f_r + \gamma, \tag{2}$$

where $F_1(v)$ is the inertial force $F_1(v)=ma_{1y}$, $\mathbf{a}=\dot{\mathbf{v}}$ and $\mathbf{v}=\dot{\mathbf{x}}$ are the acceleration and velocity of a dislocation at position $\mathbf{x}$, and B is the drag coefficient for the partial dislocations. The Peierls barrier is not included because it is negligible for fcc metals. The B for each partial is assumed equal and may be a function of $\mathbf{v}$.[3,48] m is the mass of each partial and, at high velocity, is not constant. m is calculated from its edge (b_e) and screw (b_s) components as[13]

$$m = \frac{\mu}{C}\left\{ b_e^2\left[1 + \left(\frac{C}{C_l}\right)^4\right] + b_s^2\right\}, \tag{3}$$

where $C=\sqrt{\mu'/\rho}$ is the shear wave speed, $C_l=\sqrt{\lambda+2\mu'/\rho}$ is the longitudinal wave speed, μ and λ are Lamé's constants, and ρ is the material density.

The Peach-Koehler force (per unit length) on each partial due to stress σ is calculated as

$$\mathbf{F}_{\mathrm{PK},p} = (\mathbf{b}_p \cdot \sigma) \times \xi, \quad p = 1,2. \tag{4}$$

We express the local stresses τ_{xz} and τ_{yz} as τ_x and τ_y, respectively. (These local resolved stresses would result from the applied stress and long- and short-range stresses from surrounding dislocations.) The y components of the Peach–Koehler forces on each partial are then

$$F_{\mathrm{PK},1} = b_{1x}\tau_x + b_{1y}\tau_y \tag{5}$$

and

$$F_{\mathrm{PK},2} = b_{2x}\tau_x + b_{2y}\tau_y, \tag{6}$$

where b_{1x}, b_{1y}, b_{2x}, and b_{2y} are components of $\mathbf{b}_1$ and $\mathbf{b}_2$ in the x and y directions, respectively.

Unlike perfect dislocations, each partial in the extended configuration experiences two extra forces: an attractive force per unit length γ from the energy required to create the fault and a repulsive force f_r from the interaction with the other partial. These forces act normal to the dislocation line ξ (e.g., along y in Fig. 1). The repulsive force (per unit length) is inversely proportional to the fault width w as follows:

$$f_r = \frac{A}{w}, \tag{7}$$

where A is a function of the elastic constants and the character of the partial dislocations.

For an isotropic material, A is[3]

$$A_{\mathrm{iso}} = \frac{\mu}{2\pi}\left[(\mathbf{b}_1 \cdot \xi_1)(\mathbf{b}_2 \cdot \xi_2) + \frac{(\mathbf{b}_1 \times \xi_1)\cdot(\mathbf{b}_2 \times \xi_2)}{1-\nu}\right]. \tag{8}$$

Applying Eq. (8) for a dissociated screw dislocation, A becomes

$$A_{\mathrm{iso}}^s = \frac{\mu b^2}{24\pi}\left(2 - \frac{\nu}{1-\nu}\right) \tag{9}$$

and for a dissociated edge dislocation, it is

$$A_{\mathrm{iso}}^e = \frac{\mu b^2}{8\pi}\left(\frac{1}{1-\nu} - \frac{1}{3}\right), \tag{10}$$

where ν is Poisson's ratio and $b=|\mathbf{b}|$. For an anisotropic material, A for a screw dislocation is[3]

$$A_{\mathrm{aniso}}^s = \frac{b^2}{2\pi}\left(\frac{K_s}{4} - \frac{K_e}{12}\right), \tag{11}$$

where K_s and K_e are energy coefficients as a function of anisotropic elastic constants.[3] In Eqs. (8) and (11), interactions between screw and edge are null.

B. Steady-state velocity and width

Consider the perfect screw dislocation as illustrated in Fig. 1(a) that dissociates into a lead partial $\mathbf{b}_1$ and trailing partial $\mathbf{b}_2$ separated by w in Fig. 1(b). In this case, $b_{1x}=b_{2x}=b_x=b/2$ and $b_{2y}=-b_{1y}=-b_y=-b/2\sqrt{3}$ and the equations of motion for the two partials become

$$ma_{1y} + Bv_{1y} = f_r - \gamma + (b_x\tau_x + b_y\tau_y) \tag{12}$$

and

$$ma_{2y} + Bv_{2y} = -f_r + \gamma + (b_x\tau_x - b_y\tau_y). \tag{13}$$

By adding Eqs. (12) and (13), or subtracting Eq. (13) from Eq. (12), we have, respectively,

$$m\frac{a_{1y}+a_{2y}}{2}+B\frac{v_{1y}+v_{2y}}{2}=b_x\tau_x \tag{14}$$

and

$$m\ddot{w}+B\dot{w}=2(f_r-\gamma+b_y\tau_y), \tag{15}$$

where $\ddot{w}=a_{1y}-a_{2y}$ and $\dot{w}=v_{1y}-v_{2y}$. Let

$$a=\frac{a_{1y}+a_{2y}}{2} \tag{16}$$

and

$$v=\frac{v_{1y}+v_{2y}}{2} \tag{17}$$

be the average acceleration and speed of the extended dislocation.

If the conditions are such that both partials are able to reach steady state and their steady-state velocities are equal, then $\ddot{w}=0$ and $\dot{w}=0$. In this situation, Eq. (14) becomes

$$v_{ss}=\frac{b_x\tau_x}{B}. \tag{18}$$

In other words, the steady-state velocity v_{ss} depends only on τ_x and not on τ_y. Because of this, τ_x is the driving component of τ of a screw dislocation.

With Eq. (7), Eq. (15) at steady state can be written as

$$w_{ss}=\frac{A}{\gamma-b_y\tau_y}, \tag{19}$$

where w_{ss} is the steady-state stacking fault width and either Eq. (8) or Eq. (11) can be used for A. w_{ss} depends on γ, on material constants, and on τ_y, but not on τ_x. For $\tau_y<0$, w_{ss} contracts with increasing $|\tau_y|$. A limiting value of $\tau_y<0$ can be estimated from the minimum distance $w_{\text{constrict}}$ at which the self-energies of the extended and perfect dislocations are equal.[3] For $\tau_y>0$, w_{ss} expands. In this case, $\tau_y=\gamma/b_y$ represents an upper limit for τ_y, at which a steady-state value of w cannot be achieved and partial separation increases unbounded in time. For $\tau_y=0$, $w_{ss}=w_0=A/\gamma$, regardless of dislocation speed [Eq. (18)].

C. Relativistic effects on w_{ss}

In Eqs. (8) and (11), A is independent of v. However, Weertman[8] and Hirth and Lothe[12] showed that the elastic fields of a uniformly moving dislocation change with its speed, a so-called relativistic effect. As the speed increases up to the Rayleigh wave speed C_r, the interaction force between the screw parts decreases and that between the edge parts increases. Therefore, for an extended screw dislocation, the repulsive force between the like-screw parts will decrease and the attractive force between the oppositely signed edge parts will increase, bringing the two partials together. The opposite occurs for a dissociated edge dislocation. For speeds greater than C_r, like-signed edge dislocations attract and oppositely signed ones repel. The two partials of an extended screw dislocation, for example, moving faster than C_r, will separate with speed. At C, they will tear apart.

In the event that both partials are moving at the same uniform speed v, one can approximately account for these relativistic effects on w_{ss} over the entire speed range $0\le v/C\le 1$ in a redefined $A(v)$. $A(v)$ for an extended dislocation in an isotropic material can be written from the work of Weertman[8] or Weertman and Weertman[49] as follows:

$$A(v)=\frac{\mu}{2\pi}\left[\beta_2(\mathbf{b}_1\cdot\xi_1)(\mathbf{b}_2\cdot\xi_2)+4\left(\frac{C^2}{v^2}\right)\left(\beta_1-\frac{\alpha^4}{\beta_2}\right)(\mathbf{b}_1\times\xi_1)\times(\mathbf{b}_2\times\xi_2)\right]. \tag{20}$$

For a screw dislocation, it is

$$A^s(v)=\frac{\mu b^2}{8\pi}\left\{\beta_2-\frac{1}{3}\left(\frac{C^2}{v^2}\right)[(1+\beta_2^2)^2/\beta_2-4\beta_1]\right\} \tag{21}$$

and for an edge dislocation, it is

$$A^e(v)=-\frac{\mu b^2}{8\pi}\left\{\frac{1}{3}\beta_2-\left(\frac{C^2}{v^2}\right)[(1+\beta_2^2)^2/\beta_2-4\beta_1]\right\}, \tag{22}$$

where $\beta_1^2=1-v^2/C_l^2$, $\beta_2^2=1-v^2/C^2$, and $\alpha^2=1-v^2/2C^2$.

The same result is obtained using the Lagrangian-based derivation of Hirth and Lothe,[12] although the expressions may appear in slightly different form than those of Weertman.[8]

Returning to the case in which $\ddot{w}=0$ and $\dot{w}=0$ but with relativistic effects, w_{ss} of an extended screw dislocation is instead

$$w_{ss}(v_{ss})=\frac{A(v_{ss})}{\gamma-b_y\tau_y}\equiv\frac{A(\tau_x)}{\gamma-b_y\tau_y}. \tag{23}$$

Combining Eqs. (18) and (23), w_{ss} is found to be a function of both τ_y and τ_x. For $\tau_y=0$, $w\neq w_0$ when the dislocation is moving fast under a large τ_x. This case is the same as the "no-stress" result found by Hirth and Lothe.[12]

For an edge dislocation, $b_{2x}=-b_{1x}=-b_x=-b/2\sqrt{3}$ and $b_{2y}=b_{1y}=b_y=b/2$. The steady-state velocity and stacking fault width are $v_{ss}=\frac{b_y\tau_y}{B}$ and $w_{ss}(v_{ss})=\frac{A(v_{ss})}{\gamma-b_x\tau_x}\equiv\frac{A(\tau_y)}{\gamma-b_x\tau_x}$. The dissociated edge expands with $|\tau_x|$ when $\tau_x>0$, and the critical value at which it splits infinitely apart is γ/b_x. It shrinks with $|\tau_x|$ when $\tau_x<0$.

III. MOLECULAR DYNAMICS SIMULATION MODEL OF A MOVING SCREW DISLOCATION

We use classical MD simulations to study the effect of τ_x and τ_y on w of a moving screw dislocation. For any atom i, its motion is calculated by solving Newton's second law of motion as follows:

$$m_a\ddot{\mathbf{r}}_i=\mathbf{f}_i=-\frac{\partial E}{\partial\mathbf{r}_i}, \tag{24}$$

where m_a is the mass of an atom, $\mathbf{r}$ is the position vector, $\mathbf{f}$ is the force on the atom, and E is the potential energy of the

system. In our MD simulations, we use the embedded-atom method, which was first developed by Daw and Baskes,[50] for E as follows:

$$E = \sum_{i=1}^{N} F_i(\bar{\rho}_i) + \frac{1}{2} \sum_{i \neq j, i, j=1}^{N} \phi_{ij}(r_{ij}), \tag{25}$$

where F is the embedded function, ϕ is the pairwise interaction between atoms i and j with separation distance r_{ij}, and $\bar{\rho}$ is the electron density. In this paper, the potential parameters developed by Voter[51] for copper are used. The simulations were conducted at constant temperature $T=300$ K. The material constants used in the analytical calculations are calculated from the interatomic potential: $\mu=59.8$ GPa, $\nu=0.315$, $C_l=4477.1$ m/s, $C=2587.37$ m/s, $K_e=82.1$ GPa, $K_s=47.6$ GPa, and $\gamma=0.0361$ J/m^2. This value of γ is just slightly lower than what has been calculated or measured elsewhere for Cu.[52,53] Yet, it is still comparable to Au, which is also considered an intermediate stacking fault material such as Cu. Measured partial widths for Cu and Au have been found to be approximately the same.[44] γ is higher than that for Ag, which is considered a low stacking fault energy material, and lower than that for Al, which is a common high stacking fault energy material.

The geometrical setup of the simulation block is shown in Fig. 2, with the x axis along [110], y axis along $[\bar{1}12]$, and z axis along $[1\bar{1}1]$. In the z direction, the top and bottom of the simulation block are free surfaces. In the x direction, we apply periodic boundary conditions. In the y direction, we adopted special periodic boundary conditions developed by Rodney and Martin[54] for screw dislocations. In this way, the dislocation has an infinitely long region to propagate without leaving the crystal. According to this setup, the stress field on the screw dislocation from one of its images is $\sigma_{zx} = \mu b / 2\pi y$, where y is the relative distance (+ or −) between the two. So, because of symmetry, there is no net force on the screw dislocation from its images. The edge components of the partials experience some interactions, which is negligible due to the selected large y separation (~140 b). Only under certain stress states and high-stress levels when the stacking fault can grow very wide and be close to other dislocations will there be strong effects that can significantly change the stacking fault width. As we will point out later, there is only one simulation where this is the case, prohibiting a dislocation from splitting infinitely apart, as predicted by the analytical solution when $\tau_y > \gamma / b_y$ [Eq. (23)].

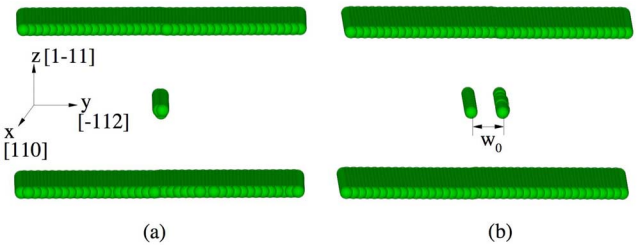

FIG. 2. (Color online) (a) The geometrical setup for the molecular dynamics simulations and the coordinate system with crystal plane orientations. A screw dislocation is inserted in the middle of the simulation block. (b) The perfect screw dislocation has split into two partial dislocations separated by width w_0. Atoms with less than 12 nearest neighbors are shown. Stacking fault width w is measured as the distance between the centers of the two partials.

The simulation volume dimensions are $5.1(x) \times 35.4(y) \times 21.3$ nm$^3(z)$ and it contains 326 400 atoms and 102 lattice planes. Different values for the z dimension were tested to study the effect of surface image forces and ensure that the predictions converge to the same values for stacking fault width. $z=21.3$ nm is found to be sufficiently large, such that within the stress limits where a dislocation is predicted to not split apart unstably, steady state is achieved and the evolution of v and w is not affected by the simulation size.

To visualize the dislocations, atoms with less than 12 first-nearest neighbors are plotted, so that only the partials and not the atoms within the stacking fault are shown. The stacking fault width is measured as the distance between the center of the two partials, as shown in Fig. 2(b). It is expected that the calculated values for w may vary if other choices are used to determine partial positions and define stacking fault width.

A screw dislocation with Burgers vector $\mathbf{b}=\frac{1}{2}[110]$ (along x) is inserted into the perfect lattice by moving all atoms

TABLE I. Normalized steady-state stacking fault width, w_{ss}/w_0, from analytical solution for different applied stresses, τ_x and τ_y (stress unit: MPa), while MD results are reported inside the parentheses.

	$\tau_y=0$	$\tau_y=-200$	$\tau_y=200$	$\tau_y=-500$	$\tau_y=500$
			A_{iso}		
$\tau_x=0$	1	0.71	1.69	0.50	∞
			A_{Aniso}		
$\tau_x=0$	1	0.71	1.69	0.50	∞
			$A(v)$		
$\tau_x=0$	1(1)	0.71	1.69	0.50	∞
$\tau_x=50$	0.97(1)	0.69	1.64	0.48	∞
$\tau_x=100$	0.89(0.95)	0.63(0.75)	1.50(1.40)	0.44(0.60)	∞(2.20)
$\tau_x=200$	0.80(0.75)	0.57(0.60[a])	1.36(1.34)	0.40(0.45)	∞
$\tau_x=500$	0.73(0.65)	0.52(0.50)	1.24(1.18)	0.36(0.30)	∞

[a]From Fig. 9.

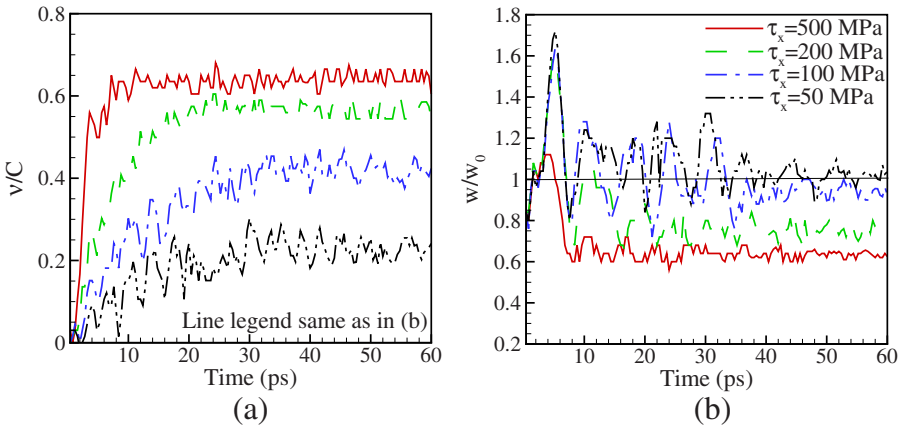

FIG. 3. (Color online) MD simulations of (a) the normalized speed of a screw dislocation and (b) the normalized stacking fault width under different τ_x and $\tau_y = 0$.

according to dislocation theory.[3] Then, the system is allowed to relax, stress-free, for 3 ps. The dislocation dissociates in the xy plane into two partials with Burgers vectors $\mathbf{b}_1$ and $\mathbf{b}_2$ with an intrinsic fault in between following

$$\tfrac{1}{2}[110] \rightarrow \tfrac{1}{6}[121] + \tfrac{1}{6}[21\bar{1}]. \tag{26}$$

The relaxed stacking fault width of the screw dislocation at the end of relaxation is about 2.0 nm, which lies in between the isotropic analytical prediction of 2.20 nm and anisotropic prediction of 1.46 nm. This is the starting configuration for all MD simulations under stress. A shear stress, $\boldsymbol{\tau}$, is applied to all atoms lying in the top and bottom surfaces of the simulation box. This relaxed stacking fault width is taken as the "static and stress-free" stacking fault width w_0, while the stacking fault width under stress will be referred as the "dynamic" stacking fault width w.

IV. RESULTS

To study the motion of the extended screw dislocation in Eq. (26), we use three types of loading in the MD simulations. In the first type, only τ_x is applied. In the second type, both τ_x and τ_y are applied. In the third type, τ_x and τ_y are initially applied, followed by a reversal of the stress. For all results, w and v are normalized by the static stacking fault width w_0 and the shear wave speed C, respectively. For comparison, the analytical predictions of w using Eq. (19) or Eq. (23) for A under these same stress states are listed in Table I. In the relativistic case [Eq. (23)], where A depends on v_{ss}, v_{ss} calculated from the MD simulations at each value of τ_x is used. As shown in Table I, the anisotropic formulation leads to a lower w than the isotropic one,[55] but the effect of anisotropy (without relativistic effects) is removed by the normalization w_0.

A. Stacking fault width under τ_x only

In this set of simulations, a wide range of τ_x are applied ($\tau_x = 50-5000$ MPa) while $\tau_y = 0$. The time evolutions of v and w are shown in Fig. 3 for $\tau_x = 50$, 100, 200, and 500 MPa. Figure 3(a) shows that the higher the τ_x, the quicker the dislocation achieves steady state and the higher the v_{ss}. For the stress levels simulated here, $v_{ss}/C > 0.2$.

The MD calculations in Fig. 4 show that v_{ss} nonlinearly varies with τ_x. v_{ss} linearly increases with stress at low stresses (at and below 100 MPa) where it can reach $\approx 0.45C$. Above this range, v_{ss} slowly increases with τ_x seeming to asymptotically approach C. Such deviations from the linear stress-velocity regime are difficult to experimentally observe,[56] and have only been observed at velocities above $0.1C$ in LiF crystals in Refs. 56–58. This asymptotic behavior has also been observed in MD simulation at different temperatures.[42] To date, the reasons for the nonlinear behavior of dislocation speed with stress are unknown.

It has been observed in experimental studies and other MD simulations that the drag coefficient B increases with temperature in agreement with many theories.[56,59–61] Therefore, it is quite possible that locally around a fast-moving dislocation, the temperature increases, thereby increasing the drag. A preliminary estimate of the temperature rise yields only 20 K over the stress range 50–500 MPa. However, estimating the local temperature rise around the core of a fast-moving dislocation is not straightforward and one should take this result as very approximate.

We explore the notion that the asymptotic behavior could be associated with a concomitant increase in B. B is estimated by applying Eq. (18) for each (τ_x, v_{ss}) and plotted in Fig. 4(b). At the lower stresses, $\tau_x \leq 100$ MPa, B is constant and equal to 22 μPa s, which is in reasonable agreement with measurements for Cu.[56,62] At higher stresses, it linearly increases with τ_x as follows:

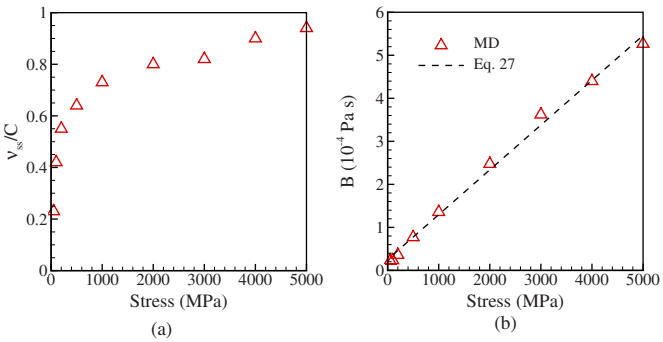

FIG. 4. (Color online) MD calculations of (a) the normalized steady-state speeds of a screw dislocation under different applied stresses τ_x; (b) the calculated drag coefficients for different applied stresses τ_x. The fitted line is Eq. (27).

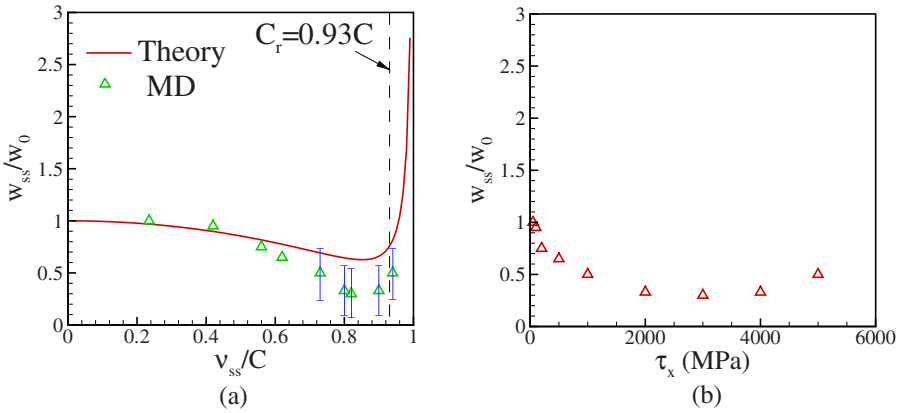

FIG. 5. (Color online) (a) Changes in the normalized steady-state stacking fault width as a function of normalized steady-state dislocation speed, showing the Weertman effect. Solid lines are from Eq. (23), and triangles are from the MD simulations. (b) Relationship between the applied τ_x and the steady-state stacking fault width w_{ss}.

$$B = K\left(\frac{b}{C}\right)\tau_x + B_0, \tag{27}$$

where $B_0=25.5$ μPa s, and $K=1.053\,35$, which is interestingly very close to unity. Note that the first term only prevails when $\tau_x > 10^2$ MPa. One should keep in mind, however, that in the linear range, B is clearly defined, while in the asymptotical range, it arguably is not. According to Eq. (18), we have v_{ss} as a function of τ_x only:

$$v_{ss} = \frac{b_x \tau_x}{K\left(\frac{b}{C}\right)\tau_x + B_0}. \tag{28}$$

Plugging this equation back to Eq. (21) for $A(v_{ss}) \equiv A(\tau_x)$ and in turn Eq. (23) for $w_{ss}(\tau_x)$, the relationship between τ_x and w_{ss} can be established and is plotted in Fig. 5(b).

With the values of B for $\tau_x=50$, 100, 200, and 500 MPa, Eq. (1) predicts that at approximately $t=28$, 27, 17, and 8 ps, respectively, the dislocation reaches 95% of its v_{ss}, which is in good agreement with the MD results.

Figure 3(b) shows the corresponding time evolution of w/w_0. Consistent with the results of other MD studies,[42] we find that w oscillates during the entire simulation with a period of a few picoseconds or less. The amplitudes of the oscillations are generally smaller for the faster-moving dislocations. The peak value w_{max} occurs in the beginning of the simulation, within 6 ps. After the steady-state velocity is reached, w continues to oscillate but at a lower amplitude. The values of w_{max} and corresponding times are listed in Table II. The time and value of w_{max} are approximately the same for $\tau_x \leq 200$ MPa and decrease with τ_x for $\tau_x > 200$ MPa.

The oscillations hinder a straightforward calculation of w_{ss}. Here, an w_{ss} is estimated from the MD simulations by averaging w/w_0 over a time interval of 10–15 ps much later after v_{ss} is achieved. Table I compares this w_{ss} with the analytical models (19) and (23). Figure 3 and Table I show that for $\tau_x=100$ MPa and higher (or for $v_{ss} \geq 0.4C$), the steady-state width contracts, that is, $w_{ss}/w_0 < 1$. Because $\tau_y=0$, this contraction is not predicted by Eq. (19) ($w/w_0=1$), which does not account for relativistic effects. The calculation of w/w_0 using $A(v)$ in Eq. (23), which does account for relativistic effects, predicts this contraction in reasonable agreement with the MD results (see first column, $\tau_y=0$ in Table I). The agreement is reasonable considering that any coupling between elastic anisotropy and relativistic effects are neglected in Eq. (23). (As mentioned earlier, anisotropic effects predicted in the stationary formulation [Eqs. (11) and (19)] have been removed in the normalization by w_0.)

One important consequence of relativistic effects, as explained by Weertman[8] and Hirth and Lothe,[12] is that when the dislocation speed exceeds the Rayleigh wave speed (here $C_r \approx 0.93C$), edge dislocations of like-sign attract and opposite-sign ones repel. Like-screw dislocations, on the other hand, do not anomalously behave in this way, at least in an isotropic material. However, the change in the interaction between the edge components with speed dominates over that between the screw components. Accordingly, the partial separation of a fast-moving extended screw dislocation will not continuously constrict with speed up to C, as the repulsion between its oppositely signed edge components will dominate and cause the stacking fault width to expand.

Figure 5 compares w_{ss} as a function of v_{ss} for $\tau_y=0$ as calculated from Eq. (23) and the MD simulations. As shown, both theory and simulation predict that w_{ss} of an extended

TABLE II. MD results of the maximum values of the stacking fault width, as w_{max}/w_0, and the time it occurred t_{max} (ps) in parentheses. Stresses are in MPa.

	$\tau_y=0$	$\tau_y=-200$	$\tau_y=200$	$\tau_y=-500$	$\tau_y=500$
$\tau_x=50$	1.7(6.0)				
$\tau_x=100$	1.6(6.0)	1.3(2.0)	2.3(5.0)	1.3(2.0)	5.2(10.0)
$\tau_x=200$	1.6(5.0)	1.8(12.0)[a]	2.1(4.0)	1.2(2.0)	
$\tau_x=500$	1.1(4.0)	1.3(2.0)	1.7(5.0)	1.3(2.0)	

[a]From Fig. 9, time measured from load reversed.

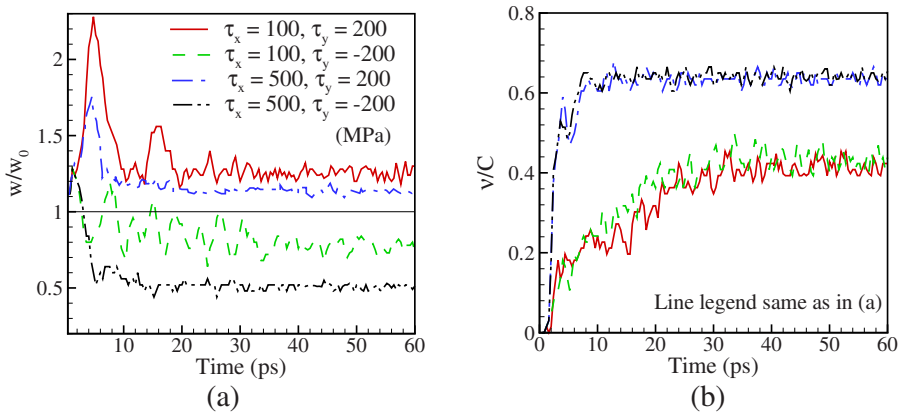

FIG. 6. (Color online) (a) The evolution of the normalized stacking fault width and (b) the normalized speed of a screw dislocation under various τ_x and $\tau_y = \pm 200$ MPa.

screw constricts with speed until $v_{ss} \approx 0.8C$. A further increase in speed over C_r causes the separation to increase toward w_0 and eventually tear apart at $v/C=1$. The agreement for the turning point velocity is not bad in spite of the isotropic assumption used in the theory. Also in both, the turning point occurs below C_r, and around C_r, w_{ss} still remains below w_0.

Generally, Eq. (23) agrees well with the MD predictions below $v_{ss}/C=0.65$, but underestimates the constriction at higher v_{ss}/C. There are several possible reasons for this discrepancy. First, we consider any errors coming from measuring the stacking fault width, which become relatively larger as the width becomes smaller (see error bars). For example, in our case when it is 50% contracted, w is less than $5b$ and therefore including or excluding one row of atoms in determining the partial positions will generate an error of about $\pm 2b$, which is more than 40% error. Despite the generous error, it still does not completely explain the discrepancy. Another reason may have to do with the assumption of isotropy. For dislocations of certain orientations in an anisotropic material (providing three displacement components), parallel screw-edge interactions may not be null and dynamic interactions between like screws and parallel screw and edge can also exhibit anomalous behavior.[63] In the present material model, the elastic constants for this dislocation orientation are $C_{11}=179$ GPa, $C_{12}=123$ GPa, and $C_{44}=81$ GPa. The anisotropy factor is $2C_{44}/(C_{11}-C_{12})=2.89$, which is relatively high. However, according to continuum theory, the dislocation in the present case $[\xi \| (110)]$ is not oriented such that three displacement components are expected.[64] Last, there is the usual consideration: The discrepancy simply results because when $w/w_0 \leq 0.5$ or $w \leq 1$ nm, the partials are too close for continuum theory to apply.

B. Stacking fault width under τ_x and τ_y

In this set of simulations, both τ_x and τ_y are nonzero. In Fig. 6, the time evolutions of w and v are plotted for $\tau_y = \pm 200$ MPa and $\tau_x=100$ or 500 MPa. In agreement with Eq. (18), v is determined by the value of τ_x, irregardless of the magnitude and sense of τ_y. Also, in agreement, when $\tau_y<0$, the stacking fault contracts and vice versa when $\tau_y>0$. For a given τ_y, w_{ss} decreases as τ_x increases. The theory without relativistic effects [Eq. (19)], however, predicts that w should be independent of τ_x, see Table I. With relativistic effects [Eq. (23)], the theory can explain the reduction in w with increase in τ_x (or velocity) observed in MD. As before, oscillations in w persist and, prior to reaching steady state, are more pronounced for the slower-moving dislocations ($\tau_x=100$ MPa).

To enhance the stress orientation effect, τ_y is increased in magnitude to ± 500 MPa, and τ_x is either 100, 200, or 500 MPa and the results are shown in Fig. 7. Again, it is observed in MD that w expands under positive τ_y and shrinks under negative τ_y. For $\tau_y=-500$ MPa, w_{ss} decreases further as velocity increases, a trend predicted by Eq. (23), which accounts for relativistic effects (see Table I), but not by Eq. (19), which neglects it.

As discussed in Sec. II, it is possible for a sufficiently high τ_y (>489 MPa for this material) to tear apart a dislocation. Due to the finite size of the MD simulation, this be-

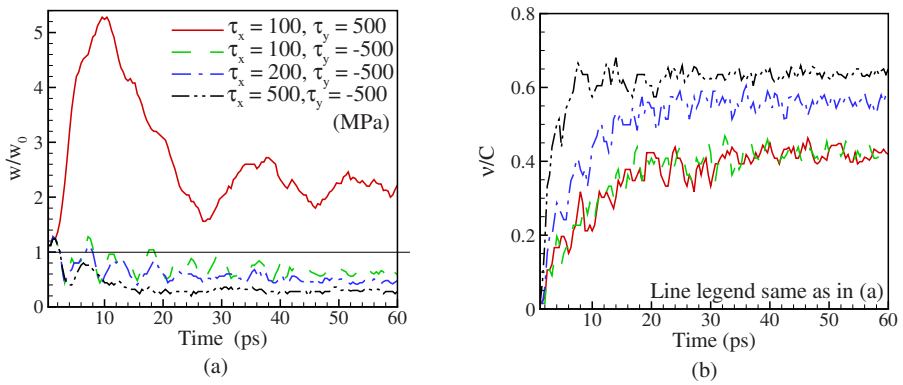

FIG. 7. (Color online) (a) The evolution of the normalized stacking fault width and (b) the normalized speed of a screw dislocation under various τ_x and $\tau_y = \pm 500$ MPa.

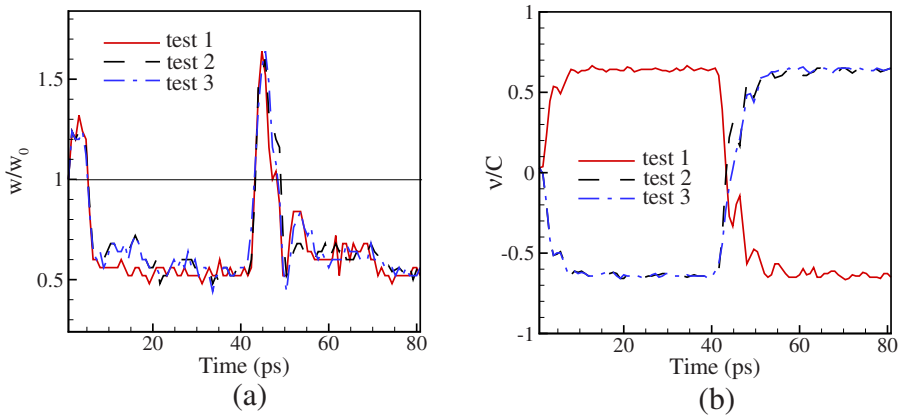

FIG. 8. (Color online) (a) The normalized stacking fault width and (b) the normalized speed of a screw dislocation under reverse loadings and τ_x only.

havior cannot be simulated, as shown in Fig. 7 for $\tau_y = 500$ MPa. As described earlier, the boundary conditions are such that we are actually simulating an array of screw dislocations, and their interactions would prohibit an unbounded expansion of w.

C. Stacking fault width under a stress reversal

Stress- and velocity-induced separation of partial dislocations suggests that interesting transient behavior may occur in the event of a strain path change. In this section, we take a preliminary look into the effect of a reversal path change on w. We first examine the influence of the reversal sequence and loading rate when $\tau_y = 0$. In test 1, we apply $\tau_x = 500$ MPa, then abruptly reverse the stress ($\tau_x = -500$ MPa) at 40 ps. Test 2 is the opposite: in the preload $\tau_x = -500$ MPa, followed by an abrupt reversal at 40 ps. In test 3, we preload again at ($\tau_x = -500$ MPa) and at 40 ps unload and reload in reverse at a rate of 100 MPa/ps.

The w and v for these three tests are compared in Fig. 8. The sign of the preload and loading rates did not affect the results. w_{ss} and v_{ss} are the same before and after the reload. Due to relativistic effects ($v/C \approx 0.6$), w_{ss} contracts to nearly half w_0 as seen earlier in Fig. 3 and Eq. (20). There is a transition period of 10 ps after the load is reversed where v changes and w expands to 1.6 times w_0. This maximum value w_{max} after the reload is much higher than w_{max} in the preload (see Table II).

Next, in Fig. 9, we examine the impact of the stress orientation effect on a reverse path change by considering $\tau_y \neq 0$. In the preload, $\tau_x = 200$ MPa, $\tau_y = 200$ MPa, which expands w_{ss} and after $t = 40$ ps, the stresses are reversed: $\tau_x = -200$ MPa, $\tau_y = -200$ MPa, which contracts w_{ss}. As before, a transition period exists, during which v and w change their values in response to the stress reversal. However, in this case, the transition period is much longer, ≈ 30 ps. In this period, w expands to a $w_{max} = 1.8$, which is much higher than w_{max} under the same state in monotonic loading. Afterward, w contracts below w_0 and achieves steady state, close to the value predicted by the model and expected under monotonic loading (see Table I).

These few examples suggest that reverse path changes can induce transient expansions of w, but no permanent effect on w_{ss}. A more complete strain-reversal analysis is deserving and left for future work.

V. DISCUSSION

A. Some interpretations and limitations of continuum dislocation theory in dynamic dislocation motion

In the present MD simulations, dislocation motion in the speed range of $0.2C < v < C$ is not strictly uniform, consisting of small local accelerations and decelerations and at best reaches a quasisteady state. First, we seek insight from comparisons with the analytical model (1). Equation (1) predicts oscillations with an amplitude of at most $w/w_0 = 1.0005$ and a period of 10–15 ps when $B = 22$ μPa s, and no oscillations when $B = 50$ μPa s. In the former case, the oscillations

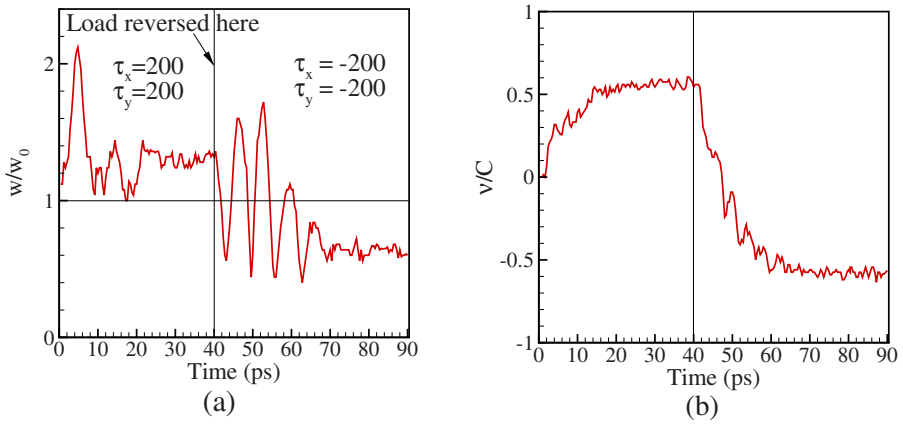

FIG. 9. (Color online) (a) The evolution of the normalized stacking fault width and (b) the normalized speed of a screw dislocation under reverse loadings of both τ_x and τ_y.

stopped after 200 ps or so. Therefore, the concomitant increase in B may explain the reduced amplitude of these oscillations with dislocation speed, but not their presence. Moreover, this comparison implies that the oscillations observed in the MD must not be attributed to any of the dynamics contained in the continuum-based equation of motion (1) (e.g., inertia, drag, and interaction between partials). Mordehai *et al.*[42] also attempted to analytically explain the oscillations, but their equation of motion did not account for the applied stress or drag. Incidentally, we find that the oscillations were not affected by the simulation size in the z direction and were not reduced when the loading rate was reduced.

The above analysis leads us to believe that the oscillations are most likely due to the discrete atomistic nature of the dislocation and its interaction with the crystal. This still opens up many other possible explanations. For instance, they could be due to oscillating damping forces (resulting from temperature fluxes, phonon radiation from the core, and back stresses from the initial period of acceleration[65]),[3,66–68] phonon waves impinging on the dislocation causing it to vibrate, irregular oscillating dislocation motion near C due to nearest neighbor exchange,[69] or nonstraight motion (zigzagging) of the dislocation, which would locally change its screw-edge character.[12,66] Regarding the latter, in all MD simulations, the dislocation remained straight. Some of these effects are expected to become more pronounced with speed, while others are expected to diminish. Further work is required to check if these explanations are consistent with the observed reduction in oscillations with increases in τ_x (or speed) seen here and in other works[42] and their persistence over long simulation periods.

Dislocation speeds in the present simulations did not appreciably exceed C_r. In Ref. 42, it was possible to achieve a speed of C with an applied stress of 4000 MPa; however, in the present work, the dislocation still remains subsonic at $\tau_x = 5000$ MPa due to the increasing damping forces with speed. Whether a dislocation can move at and above C still remains a controversial subject. According to linear elastic dislocation theory, the energies of screw and edge dislocations become infinite at C for isotropic metals and at lower values for anisotropic metals.[8–11,49,63] Furthermore, it has been predicted that at high velocities near C, edge dislocations can become unstable with respect to zigzagging in isotropic metals,[3,12] and both edge and screw in anisotropic ones.[66] One- and two-dimensional discrete lattice models, in which the singularities of continuum solutions would not occur, also predict breakdown of regular dislocation motion (in adjacent planes in the 2D models) and core instabilities at speeds close to but below C,[69–71] while others do not.[67,68] One possible issue with the above works is that they do not consider all possible damping mechanisms. In this regard, a discussion by Gilman[48] proposes that dislocation speeds are limited to the subsonic regime due to viscous and inertial losses at its core.

B. High-rate and high-stress deformation

It is important to emphasize that the results of this work are important only for conditions involving high values of τ_x and τ_y, where both relativistic and orientation effects can appreciably change w from w_0. Such situations can occur in high-rate loading, shock conditions, and high-stress situations, such as near cracks, defects, and grain boundaries (particularly in nanocrystalline metals).

Partial emission can be related to the critical stress at which a dislocation will be split apart (either $\tau_{y,c}$ for a screw dislocation or $\tau_{x,c}$ for an edge dislocation).[3] In the case of a screw dislocation when $\tau_y > \tau_{y,c}$, w, according to Eq. (23), continuously expands in time as long as the stress remains constant and is not removed. Each partial achieves a different steady-state velocity and, hence, w_{ss} grows unbounded in time. As they propagate, they create stacking faults into less-stressed regions, where they can attain a finite separation. In the case of shock along the [100] direction ($\tau_y > 0$), generation of stacking faults near the shock front has been observed in very large scale MD simulations.[33] These faults propagated either forward with the front or back into the shocked material. Later, when the rarefaction wave passed, the stacking faults were removed. Based on our stress-reversal simulations, it is possible that they contracted under the reverse stress state.

When $\tau_y < \tau_{y,c}$, the dislocations in our simulations were able to achieve (quasi-) steady-state motion. However, under actual extreme conditions, it is possible that steady state is not achieved. For this reason, we also examined the peak value of stacking fault width w_{max}, which manifests in the initial transient period under constant applied stress and stress reversals (Table II). Generally, we find that w_{max}/w_0 is greater than unity in all cases and, not surprisingly, greater when $\tau_y > 0$ than when $\tau_y < 0$. w_{max} manifests from the oscillations in w and therefore the significance of w_{max} is uncertain until the reason for the oscillations is uncovered.

In the case of a cracked crystal, twins or stacking faults can be emitted from the crack tip, which changes the shape of the plastic zone ahead of it. For instance, our results are consistent with observations of dislocations (screw or mixed) in plastic zones ahead of a crack in Ni.[27] As in other metals with low to moderate γ, Ohr and co-workers[27,72,73] observed plastic zones in Ni consisting of partial dislocations. In particular, this type of plastic zone developed only in certain crack orientations, which was realized as a stress orientation effect by Kobayashi and Ohr.[27] When the tensile axis was oriented along the [001] direction ($\tau_y < 0$), no stacking faults were observed (suggesting cross slip), but along the [111] and [101] directions ($\tau_y > 0$) they were (suggesting little to no cross slip). Metals with high γ, on the other hand, generated the classical butterfly plastic zone as a result of cross slip, regardless of orientation.

C. Implications on cross slip

The likelihood a screw segment cross slips can be determined by an activation energy calculated from the energies for each event in the cross-slip process, starting with its constriction and ending with its expansion on the cross-slip plane. This energy barrier would, undoubtedly, depend on w_p, its width on the primary plane and w_c, its width on the cross-slip plane. Take, for example, the expression by

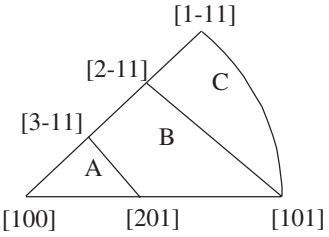

FIG. 10. Stereographic triangle for the example discussed in Sec. V.

Püschl[17] for the energy change associated with cross slip:

$$\Delta E = E_h + E_h^* + L[E(w_p) - E(w_c)], \tag{29}$$

where E_h and E_h^* are the energies to bend the dislocation for constriction on the primary plane and to bow out the dislocation expanding on cross-slip plane, L is the length of the segment that has cross slipped, and $E(w_p)$ and $E(w_c)$ are the energies associated with reducing the stacking fault on the primary plane and cross-slip planes, respectively. In theory, $E(w)$ is usually found to be proportional to w.[5,7,17] Accordingly, even without an exact expression for $E(w)$, it can be expected that cross slip will be energetically favorable when w_p is small and w_c is large and the difference $(w_c - w_p)$ is positive.[7]

Estimates for w_p and w_c can be approximated using the steady-state value in Eq. (23), where w_{ss} is a function g of τ_x, τ_y, and γ. Because τ_x and τ_y change as the screw dislocation transitions from the primary glide plane to the cross-slip plane, so will its w_{ss} and v_{ss} according to Eqs. (23) and (18).

Suppose an axial stress $\pm\sigma$ is applied along direction θ. In this loading situation, w_{ss} will be observed to vary as a function h of θ, σ, and γ as follows:

$$w_{ss} = g(\tau_x, \tau_y, \gamma) \equiv h(\theta, \sigma, \gamma). \tag{30}$$

It is straightforward to find τ_x and τ_y given θ and σ and therefore to convert from one function to another. Implicit in both expressions in Eq. (30) is the additional dependence on $v_{ss}(\tau_x)$, which arises from relativistic effects.

For this type of loading, it is natural to consider a stereographic triangle, such as the one in Fig. 10. Copley and Kear[5] defined regions in this triangle where w_p widens or narrows with stress. For tensile loading, orientations in region A would lead to a narrowing w_p with stress and orientations in region B+C, a widening w_p with stress. For orientations lying along the $[3\bar{1}1]-[201]$ boundary, there is no orientation effect because, as Copley and Kear[5] pointed out, the Schmid factors on each partial are equal for orientations along this boundary. Later, Bonneville and Escaig[7] defined three regions: A, B, and C based on the narrowing-widening behavior of both w_p and w_c. Narrowing or widening was determined by the sign of τ_y: τ_y on the primary plane changes sign across the $[3\bar{1}1]-[201]$ boundary, whereas on the cross-slip plane it changes sign across the $[2\bar{1}1]-[101]$ boundary. Consequently, tensile loads in region A lead to narrowing of w_p and w_c, in region B to widening of w_p but narrowing of w_c, and in region C to widening of w_p and w_c. Compression along these same directions has the opposite effect. Cross slip, therefore, becomes more favorable in region B as the compression stress increases.[7]

Our formulation for w_{ss} without relativistic effects [Eq. (19)] is also based solely on τ_y, and therefore will lead to the same conclusions as Bonneville and Escaig.[7] Even the analysis of Copley and Kear,[5] which is based on Schmid factors, would produce the same results as Eq. (19), which is based on PK forces, as shown by Nabarro.[4] With relativistic effects, however, we find from Eq. (23) that there is still a slight orientation effect via τ_x along the $[3\bar{1}1]-[201]$ boundary.

As an example, consider a screw dislocation with Burgers vector $\frac{1}{2}[1\bar{1}0]$ that cross slips from its primary $[111]$ plane to its cross-slip plane $[11\bar{1}]$ through an obtuse angle (or to $[\bar{1}\bar{1}1]$ through an acute angle). In this case, $\mathbf{b}_1 = \frac{1}{6}[1\bar{2}1]$ and $\mathbf{b}_2 = \frac{1}{6}[2\bar{1}\bar{1}]$ on the primary plane and $\mathbf{b}_{1,c} = \frac{1}{6}[1\bar{2}\bar{1}]$ and $\mathbf{b}_{2,c} = \frac{1}{6}[2\bar{1}1]$ on the cross-slip plane. Figure 11 compares the change in w_p/w_0 and w_c/w_0 with absolute value of σ/μ for

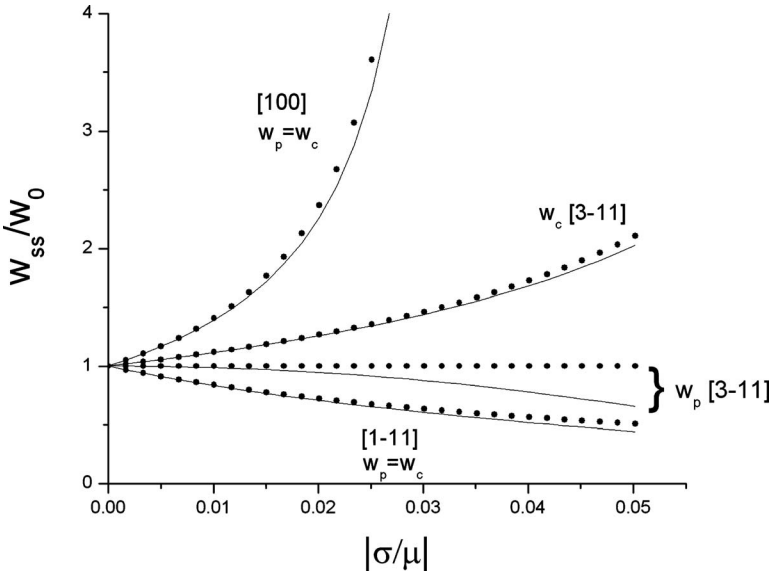

FIG. 11. Stress orientation effects on the steady-state stacking fault width (normalized by the zero-stress value w_0) in the primary w_p and cross-slip w_c planes for three compression loading orientations. The solid curves account for relativistic effects and the dotted curves do not.

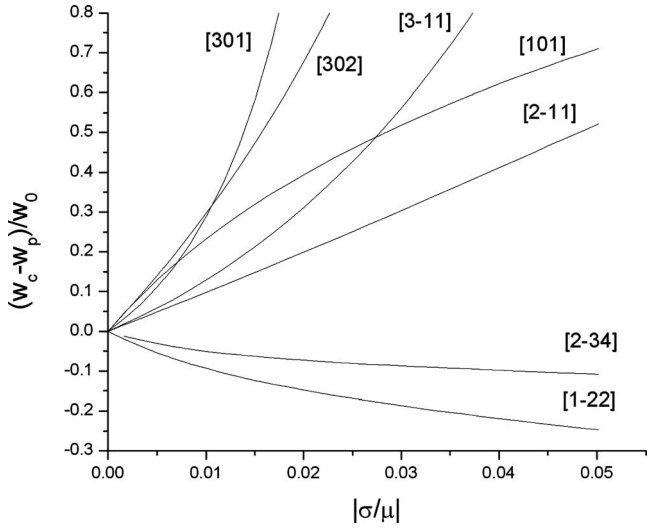

FIG. 12. The difference in the steady-state stacking fault width between the primary and cross-slip planes for several compression loading orientations as it varies with applied stress σ. These calculations account for relativistic effects.

compressive loading along orientations [100], $[3\bar{1}1]$, and $[1\bar{1}1]$, with and without relativistic effects, Eq. (23) (solid) and Eq. (19) (dots), respectively. As shown, compressive loading along the [100] direction (region A) widen both w_p and w_c, whereas loading along the $[1\bar{1}1]$ direction (region C) narrow them. Tensile loading along these same directions would have the opposite effect. Widening occurs at a faster rate than narrowing, whether it occurs under tensile loading for $[1\bar{1}1]$ or compressive loading for [100]. Relativistic effects cause the width to be slightly smaller than without. Orientations along the $[3\bar{1}1]$–[201] boundary are most affected by relativistic effects. Without them, there is no orientation effect on the primary plane, i.e., $w_p=w_0$, because τ_y is zero. With them, there is a shrinking of w_p as σ (or velocity) increases. With or without, w_c widens. Therefore, due to relativistic effects, orientations along the $[3\bar{1}1]$–[201] boundary favor cross slip under compressive loading.

Figure 12 shows $(w_c-w_p)/w_0$ with relativistic effects[74] [Eq. (23)] as a function of the absolute value of σ/μ for compression loading along several orientations: [301] in region A; boundary orientations $[3\bar{1}1]$, $[2\bar{1}1]$, and [101]; [302] in region B; and $[1\bar{2}2]$ and $[2\bar{3}4]$ in region C.

In all cases, values for w on the primary and cross-slip planes become more disparate as stress increases. $w_c>w_p$ in every orientation, except $[1\bar{2}2]$ and $[2\bar{3}4]$, where $w_c<w_p$. Tensile loading has the opposite effect.

For orientations on either side of (e.g., [301] and [302]) or along the $[3\bar{1}1]$–[201] boundary, the difference increases at a relatively faster rate with stress. This occurs because widening on the cross-slip plane in these cases rapidly grows with stress.

For orientations along the $[2\bar{1}1]$–[101] boundary, both τ_x and τ_y are zero on the cross-slip plane and therefore neither orientation nor relativistic effects can affect $w_c=w_0$. In these cases, $(w_c-w_p)/w_0$ reflects the shrinking of w_p with stress.

For the two orientations in region C, the change in w during cross slip is the least. Both w_p and w_c narrow in region C and narrowing happens at a slow rate.

For loading directions [100] and $[1\bar{1}1]$, at the extreme ends of regions A and C, respectively, $(w_p-w_c)/w_0$ is zero because $w_p=w_c$. In these cases, the last term in Eq. (29) would disappear.

In the high-velocity regime of interest here, cross slip is a dynamic process and, thus, the energetic expression should also include the associated change in kinetic energy. At this stage, we only mention changes in v_{ss} when the screw dislocation cross slips. For orientations within A and B, there is a drop in v_{ss} due to a reduction in τ_x from the primary to the cross-slip plane. The reduction is greatest for the orientations within region B. Within region C, however, v_{ss} increases from the primary to the cross-slip plane. The associated change in kinetic energy may affect the energetics of cross slip at high rates.

VI. CONCLUDING REMARKS AND RECOMMENDATIONS

Our MD results indicate that the stacking fault width of a moving screw dislocation depends not only on material constants (μ, $\mathbf{b}_1$, $\mathbf{b}_2$, and γ), but also on the applied stress and its speed. The stress orientation effect,[4,5] that is, the expansion or constriction of w relative to w_0 with changes in the magnitude and sense of τ_y, is clearly demonstrated. Most importantly, the present work indicates that in addition to this effect, w_{ss} of a screw dislocation decreases as its velocity increases, as a result of relativistic effects.[49]

The results of this study can explain some of the results reported in other MD simulation studies. In Ref. 42, the moving screw dislocation was observed to increase in width as the stress increased. This is a stress orientation effect because the stress was applied normal to the dislocation line, i.e., $\tau_y\neq 0$, and not a relativistic effect as they suggest. In fact, for speeds below C_r, the relativistic effect tends to shrink w, and not expand it. In Ref. 43, an increasing (forward) then decreasing (reverse) constricting stress was applied to a screw dislocation. The partial separation-stress curve followed a lower path in reverse than forward. It is unknown if the reported widths were steady-state values at each loading and unloading stress. If not, then the longer transient after a reversal may explain the observed hysteresis.

Examples in Figs. 11 and 12 clearly show that stress orientation effect on w_{ss} becomes significant: (1) close to the limiting values of τ_y defined by Eq. (23) or Eq. (19) and (2) for orientations away from the $[3\bar{1}1]$–[201] and $[2\bar{1}1]$–[101] boundaries, and (3) when τ_x is high, such that relativistic effects can cause a shrinkage of w, regardless of loading orientation. Relativistic effects are most noticeable for loading directions along the $[3\bar{1}1]$–[201] boundary and absent along the $[2\bar{1}1]$–[101] boundary. Otherwise, for low values of τ_x and τ_y, orientation effects are negligible, and the speeds are low, so relativistic effects are negligible as well.

Regarding cross slip, Figs. 11 and 12 show that loading orientations near the $[3\bar{1}1]$–[201] boundary or in between

the $[3\bar{1}1]-[201]$ and $[2\bar{1}1]-[101]$ boundaries (region B) that cause pronounced narrowing-widening behavior,[7] and large reductions in velocity (kinetic energy) are likely to be the most energetically favorable for cross slip. At high speeds where relativistic effects become important, even orientations on the $[3\bar{1}1]-[201]$ boundary can favor cross slip. Orientations near $[1\bar{1}1]$ where w quickly contracts with applied compressive stress on the primary plane are not necessarily favorable for cross slip because they also lead to contraction on the cross-slip plane.

It is shown that linear elastic straight dislocation theory including both stress orientation and relativistic effects can explain the dynamical contraction or expansion observed in MD simulations. The advantage is that reasonably accurate and simple expressions for w_{ss}, accounting for both effects, can be written; see, for instance, Eq. (23). These analytic expressions can benefit higher length-scale calculations, such as DD simulations. In DD simulations, the local stress state τ, motion, and orientation of every dislocation segment can be calculated as a result of the applied stress and the collective motion of the surrounding dislocations. To date, these dislocations have been assumed to be perfect, and as discussed in Sec. I, this means that many elementary dislocation processes are neglected. Use of Eq. (23) could improve the numerical treatment of dislocation interactions, reactions, and cross slip. They can provide an approximation of the instantaneous width for any given dislocation segment, assuming sufficient time is given to reach steady state in each increment and the stress states are relatively uniform across the width. Under conditions where the dislocation does not tear apart ($\tau_y < 489$ MPa in our case), the steady-state widths and speeds are achieved relatively fast, within 11–45 ps, and over short distances, within 18–46 nm.

ACKNOWLEDGMENTS

This work was supported by the Advanced Simulation and Computing Program at Los Alamos National Laboratory (LANL). LANL is operated by the Los Alamos National Security, LLC, for the National Nuclear Security Administration of the U.S. Department of Energy under Contract No. DE-AC52-06NA25396.

*zhiqiang@lanl.gov

[1] F. R. N. Nabarro, Adv. Phys. **1**, 269 (1952).
[2] G. Leibfried and H. D. Dietze, Z. Phys. **131**, 113 (1951).
[3] J. P. Hirth and J. Lothe, *Theory of Dislocations* (Kreiger, Malabar, FL, 1992).
[4] F. R. N. Nabarro, Philos. Mag. **14**, 861 (1966).
[5] S. M. Copley and B. H. Kear, Acta Metall. **16**, 227 (1968).
[6] F. R. N. Nabarro, Philos. Mag. **42**, 213 (1951).
[7] J. Bonneville and B. Escaig, Acta Metall. **27**, 1477 (1979).
[8] J. Weertman, in *Response of Metals to High Velocity Deformation*, edited by P. G. Shewmon and V. F. Zackay (Interscience, New York, 1961).
[9] F. C. Frank, Proc. Phys. Soc., London, Sect. A **62**, 131 (1949).
[10] J. D. Eshelby, Proc. Phys. Soc., London, Sect. A **62**, 307 (1949).
[11] G. Leibfried and H. D. Dietz, Z. Phys. **126**, 790 (1949).
[12] J. P. Hirth and J. Lothe, in *Dislocation Dynamics*, edited by A. R. Rosenfield, G. T. Hahn, A. L. Bement, Jr., and R. I. Jaffee (McGraw-Hill, New York, 1967), pp. 231–254.
[13] J. P. Hirth, H. M. Zbib, and J. Lothe, Modell. Simul. Mater. Sci. Eng. **6**, 165 (1998).
[14] J. J. Gilman, Mater. Sci. Eng., A **319-321**, 84 (2001).
[15] G. Saada, Mater. Sci. Eng., A **137**, 177 (1991).
[16] W. Püschl and G. Schoeck, Mater. Sci. Eng., A **164**, 286 (1993).
[17] W. Püschl, Prog. Mater. Sci. **47**, 415 (2002).
[18] M. S. Duesbery, N. P. Louat, and K. Sadananda, Acta Metall. Mater. **40**, 149 (1992).
[19] T. Rasmussen, K. W. Jacobsen, T. Leffers, O. B. Pedersen, S. G. Srinivasan, and H. Jonsson, Phys. Rev. Lett. **79**, 3676 (1997).
[20] A. N. Stroh, Proc. Phys. Soc. London, Sect. B **67**, 427 (1954).
[21] A. Seeger, Z. Naturforsch. B **9** 856 (1954).
[22] Z. Q. Wang, I. J. Beyerlein, and R. LeSar, Modell. Simul. Mater. Sci. Eng. **15**, 675 (2007).
[23] A. H. Cottrell, *Dislocations and Plastic Flow in Crystals* (Oxford University Press, Oxford, 1953).
[24] B. Escaig, in *Dislocation Dynamics*, edited by A. R. Rosenfield, G. T. Hahn, A. L. Bement, Jr., and R. I. Jaffee, (McGraw-Hill, New York, 1968), pp. 655–677.
[25] P. J. Jackson, Scr. Metall. **17**, 199 (1983).
[26] P. J. Jackson, Mater. Sci. Eng. **57**, 39 (1983).
[27] S. Kobayashi and S. M. Ohr, J. Mater. Sci. **19**, 2273 (1984).
[28] A. Abel and H. Muir, Philos. Mag. **27**, 585 (1973).
[29] W. L. Phillips, Jr. and W. D. Robertson, Trans. Metall. Soc. AIME **212**, 406 (1958).
[30] J. P. Hirth, J. Appl. Phys. **32**, 700 (1961).
[31] T. Jøssang, J. P. Hirth, and C. S. Hartley, J. Appl. Phys. **36**, 2400 (1965).
[32] T. Malis, K. Tangri, and D. J. Lloyd, Metall. Trans. A **6A**, 932 (1975).
[33] B. L. Holian and P. S. Lomdahl, Science **280**, 2085 (1998).
[34] S. Ishioka, J. Appl. Phys. **46**, 4271 (1975).
[35] V. Yamakov, D. Wolf, S. R. Phillpot, A. K. Mukherjee, and H. Gleiter, Nat. Mater. **1**, 45 (2002).
[36] X. Z. Liao, F. Zhou, E. J. Lavernia, D. W. He, and Y. T. Zhu, Appl. Phys. Lett. **83**, 5062 (2003).
[37] J. Wang and H. Huang, Appl. Phys. Lett. **85**, 5983 (2004).
[38] L. P. Kubin, G. Canova, M. Condat, B. Devincre, V. Pontikis, and Y. Brechet, Solid State Phenom. **23-24**, 455 (1992).
[39] N. M. Ghoniem, S. H. Tong, and L. Z. Sun, Phys. Rev. B **61**, 913 (2000).
[40] Z. Q. Wang, I. J. Beyerlein, and R. LeSar, Philos. Mag. **87**, 2263 (2007).
[41] S. Aubry and D. A. Hughes, Phys. Rev. B **73**, 224116 (2006).
[42] D. Mordehai, Y. Ashkenazy, I. Kelson, and G. Makov, Phys. Rev. B **67**, 024112 (2003).
[43] M. S. Duesbery, Modell. Simul. Mater. Sci. Eng. **6**, 35 (1998).
[44] T. Rasmussen, K. W. Jacobsen, T. Leffers, and O. B. Pedersen,

Phys. Rev. B **56**, 2977 (1997).
[45] T. Kinoshita, K. Kawamura, and T. Mashimo, in *Shock Compression of Condensed Matter*, edited by M. D. Furnish, M. Elert, T. P. Russell, and C. T. White (AIP, New York, 2006), pp. 395–398.
[46] J. Engbaek, J. Schiotz, B. Dahl-Madsen, and S. Horch, Phys. Rev. B **74**, 195434 (2006).
[47] X. L. Ma and W. Yang, Nanotechnology **15**, 449 (2004).
[48] J. J. Gilman, Metall. Mater. Trans. A **31A**, 811 (2000).
[49] J. Weertman and J. R. Weertman, in *Dislocations in Solids*, edited by F. R. N. Nabarro (North-Holland, Amsterdam, 1980), Vol. 3, pp. 1–60.
[50] M. S. Daw and M. I. Baskes, Phys. Rev. B **29**, 6443 (1984).
[51] A. F. Voter, Los Alamos Unclassified Technical Report No. LA-UR-93-3901, 1993.
[52] N. Bernstein and E. B. Tadmor, Phys. Rev. B **69**, 094116 (2004).
[53] N. M. Rosengaard and H. L. Skriver, Phys. Rev. B **47**, 12865 (1993).
[54] D. Rodney and G. Martin, Phys. Rev. Lett. **82**, 3272 (1999).
[55] L. J. Teutonico, Acta Metall. **11**, 1283 (1963).
[56] E. Nadgornyi, Prog. Mater. Sci. **31**, 1 (1988).
[57] J. Cotner and J. Weertman, Discuss. Faraday Soc. **38**, 229 (1964).
[58] W. G. Johnston and J. J. Gilman, J. Appl. Phys. **30**, 129 (1959).
[59] G. Leibfried, Z. Phys. **127**, 344 (1950).
[60] J. D. Eshelby, Proc. R. Soc. London, Ser. A **197**, 396 (1949).
[61] W. P. Mason, J. Acoust. Soc. Am. **32**, 458 (1960).
[62] K. M. Jassby and T. Vreeland, Scr. Metall. **5**, 1007 (1971).
[63] L. J. Teutonico, Phys. Rev. **127**, 413 (1962).
[64] To explain the observed results, additional displacement components would need to occur near the core and the resulting velocity range of anomalous behavior between like screws would have to be larger than that between edges. In support, calculations by Van Hull and Weertman (Ref. 75) show that anisotropy has the tendency to reduce the anomalous region for like edges. Calculations by Teutonico (Ref. 63) suggest that in anisotropic media, this anomalous region can be equally as broad and lie at a lower velocity range for like screws than for like edges.
[65] These oscillations may have to do with the dislocation motion in accelerating to steady state. As discussed by Hirth and Lothe (Ref. 3) and Beltz *et al.* (Ref. 66), a change in speed is associated with a change in stress state ahead of the dislocation, which creates a "back stress" on the core. As seen in Fig. 3, the higher the τ_x, the larger the B and the shorter the time period to reach (quasi-) steady state. Therefore, the fastest dislocations move at their final v_{ss} for most of the time, and any effects of a back stress may be reduced. This would mean that slower loading rates, which increase the time to each v_{ss}, would lead to larger oscillations. A preliminary check on a single case supports this.
[66] R. J. Beltz, T. L. Davis, and K. Malen, Phys. Status Solidi **26**, 621 (1968).
[67] V. Celli and N. Flytzanis, J. Appl. Phys. **41**, 4443 (1970).
[68] W. Atkinson and N. Cabrera, Phys. Rev. **138**, A763 (1965).
[69] J. H. Weiner and M. Pear, Philos. Mag. **31**, 679 (1975).
[70] S. Ishioka, J. Phys. Chem. Solids **36**, 427 (1975).
[71] Y. Y. Earmme and J. H. Weiner, Phys. Rev. Lett. **31**, 1055 (1973).
[72] S. M. Ohr and J. Narayan, Philos. Mag. A **41**, 81 (1980).
[73] S. Kobayashi and S. M. Ohr, Scr. Metall. **15**, 343 (1981).
[74] Indeed, the difference $(w_c - w_p)/w_0$ would most likely not be found in any theoretical expression for the energetics of cross slip (Refs. 15 and 17) simply because the $E(w)$ to undissociate a screw dislocation is usually a nonlinear function in w. $(w_c - w_p)/w_0$ is merely examined here to facilitate a discussion on stress orientation and relativistic effects on the likelihood of cross slip.
[75] A. Van Hull and J. Weertman, J. Appl. Phys. **33**, 1636 (1962).